INORGANIC CHEMISTRY
FRONTIERS

RESEARCH ARTICLE

Cite this: *Inorg. Chem. Front.*, 2020, **7**, 1437

Guest effects on crystal structure and phosphorescence of a Cu_6L_3 prismatic cage†

Zhi-Chun Shi,‡[a,b] Wei Chen,[b] Shun-Ze Zhan,[b] Mian Li,[b] Mo Xie,[a] Yan Yan Li,[a] Seik Weng Ng,[c] Yong-Liang Huang,[a] Zhiyin Zhang,[a] Guo-Hong Ning *[a] and Dan Li *[a]

Received 3rd December 2019,
Accepted 26th January 2020

DOI: 10.1039/c9qi01578g

rsc.li/frontiers-inorganic

Coordination cages with a nanocavity can encapsulate various guests, which allows modulation of the physical and chemical properties of the host–guest inclusion complexes. In this work, we designed and prepared a phosphorescence Cu_6L_3 trigonal prismatic cage, which accommodates a series of aromatic guest molecules. Single crystal X-ray analysis revealed that the intermolecular Cu···Cu distance can be mediated by changing the volume of the guests. Moreover, the host–guest charge-transfer interactions can be also fine-tuned *via* tailoring the ionization potential of guests. Consequently, we have observed the guest-induced photoluminescence properties change including a gradual red shift of the maximum emission peak and a linear relationship between the quantum yield and ionization potential of guests.

Introduction

Supramolecular metallacycles and metallacages with nanocavities formed through metal-directed self-assembly have been extensively investigated due to their intriguing properties that are attractive for fundamental studies as well as advanced applications.[1–5] Owing to the confined cavity of the coordination cages, one of the biggest advantages is the rich host–guest chemistry that allows modification of the photophysical and photochemical properties as well as the reactivities of hosts or guests.[1–7] Among these functionalized coordination complexes, not only the synthetic approaches for constructing fluorescent metallacycles and metallacages, but also the strategies for tuning their photoluminescence properties have been well established by Fujita,[8] Stang,[7,9,10] Nitschke,[11–13] Würthner,[14] and others.[15–20] However, phosphorescence analogues are still unexplored and the modulation of their photophysics remains challenging.[21–25]

The cyclic trinuclear complexes (CTCs) containing d^{10} coinage-metal ions, Au(I), Ag(I) and Cu(I), often exhibit bright photoluminescence due to their metal–metal charge transfer excited states and the formation of excimers or exciplexes.[26] It is well-known that the intermolecular M···M distance (M = Au, Ag or Cu) in the excimers can hugely influence their photoluminescence properties. For example, Omary *et al.* reported that variation of the substituents on the pyrazolate ligand was able to mediate the crystal packing of Cu_3Pz_3-type CTCs (Pz = pyrazolate ligand) resulting in the modulation of their photophysics.[27] Our group also observed that a bright photoluminescent CTC, Cu_3(4-chloropyrazolate)$_3$, can display different emission properties when the crystal packing alters.[28]

Inspired by the unique phosphorescence of CTCs, we envisioned that a cyclic trinuclear unit could serve as a building block to construct phosphorescent coordination cages. In 2011, the Thiel group reported a Cu_6L_3 (L = 2,2′-di(1,2-pyrazol-3-yl)-1,1′-binaphthyl) cage containing Cu_3Pz_3-type CTC units, showing fluorescence with a lifetime less than 1 ns. This is because the large steric hindrance of the pyrazolate ligand leads to a loose packing of the Cu_6L_3 cage unit with a long intermolecular Cu···Cu distance in the solid-state.[29] At the same time, our group have reported the first example of a phosphorescent Cu_6L_3 (L = *p*-xylylene-bis(3,5-dimethyl)pyrazol-4-yl) cage based on Cu_3Pz_3-type CTC units.[30] Unfortunately, due to the short intramolecular Cu···Cu distance between two CTC units and small intrinsic cavity, the encapsulation of guest molecules is unsuccessful (Scheme 1). Recently, we prepared a new phosphorescent Cu_6L_3 (L = 4,4′-thiophene-bis-methylene-bis(3,5-dimethyl)pyrazol-4-yl) cage with a cavity of

[a]*College of Chemistry and Material Science, Jinan University, Guangzhou 510632, P. R. China. E-mail: guohongning@jnu.edu.cn, danli@jnu.edu.cn*
[b]*Department of Chemistry and Key Laboratory for Preparation and Application of Ordered Structural Materials of Guangdong Province, Shantou University, Shantou 515063, P. R. China*
[c]*UCSI University, 1 Jalan Puncak Menara Gading, UCSI Heights, 56000 Cheras, Kuala Lumpur, Malaysia*

†Electronic supplementary information (ESI) available. CCDC 1963722 and 1963726–1963732. For ESI and crystallographic data in CIF or other electronic format see DOI: 10.1039/c9qi01578g

‡Present address: Department of Chemistry and Biochemistry and Biomolecular Sciences Institute, Florida International University, Miami, Florida 33199, USA.

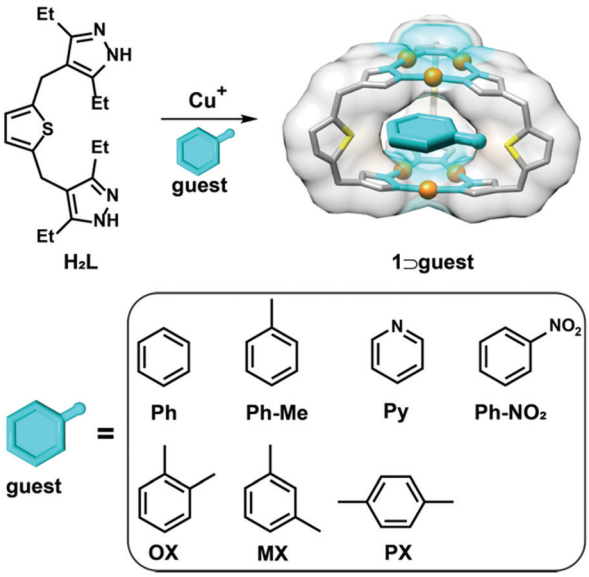

Scheme 1 Conceptual representation of the synthesis of inclusion complexes from Cu_6L_3 cage host **1** and various aromatic guests (ethyl substituent groups on pyrazole rings are omitted for clarity).

232 Å^3, which is able to encapsulate benzene and toluene molecules.[31] However, systematic studies of the effects of guest encapsulation on the crystal structures and phosphorescence of the cage hosts need to be explored.

Herein, we synthesize a phosphorescent trigonal prismatic Cu_6L_3 cage **1**, from the self-assembly of bispyrazolyl ligand H_2L (L = 4,4′-thiophene-bismethylene-bis(3,5-diethyl)pyrazol-4-yl) and Cu(I) ions. By replacement of the benzene motif with a thiophene core, the cavity of cage **1** enlarges to larger than 200 Å^3 allowing the accommodation of various aromatic guest molecules (Scheme 1). The single-crystal X-ray diffraction analysis of eight inclusion complexes confirmed that the intermolecular Cu···Cu distance increased with the increase in the guests' volume. In addition, the host–guest charge-transfer (CT) interactions can be also fine-tuned by controlling the ionization potential (IP) of the guest. Through regulating the combined effects of the cuprophilic interaction and host–guest CT processes on the photophysical properties of the inclusion complexes, we achieve tunable photoluminescence properties of coordination cages by host–guest modulation.

Results and discussion

Guest selection

M_3Pz_3-type (M = Au, Ag and Cu) complexes are able to bond π-acidic as well as π-basic molecules to form the donor–acceptor adducts, as a result, photoluminescence properties of M_3Pz_3 complexes can be tuned.[32] In addition, recent theoretical and experimental studies revealed that the relative π-basicity of Cu_3Pz_3-type CTCs is stronger than Ag_3Pz_3-type CTCs, but weaker compared to Au_3Pz_3-type CTCs.[32–34] Inspired by this, we assumed that the metal–organic cage host composed from Cu_3Pz_3 could encapsulate either electron-rich or -poor aromatic guests and its photophysical properties can be mediated by the introduction of guests with different electronic properties. Thus, a series of benzene derivatives with different substituents (*i.e.*, benzene (**Ph**), *o*-xylene (**OX**), *m*-xylene (**MX**), *p*-xylene (**PX**), toluene (**Ph-Me**), pyridine (**Py**), and nitrobenzene (**Ph-NO$_2$**)) have been chosen to test our hypothesis (Scheme 1). For comparison, an inclusion adduct with a non-aromatic guest, dichloromethane (**DCM**), was also prepared.

Preparation of host–guest inclusion adducts and general characterization

Colorless single crystals of host–guest complexes were obtained from solvothermal reactions in a mixture of Cu_2O, H_2L, acetonitrile, and corresponding aromatic guests (Scheme 1). The experimental details are given in the ESI.† It is worthy to mention that the Cu_6L_3 cage crystals could not be obtained in the absence of aromatic guests, indicating the guests act as a template to assist the formation of the Cu_6L_3 cage. High-quality single crystals suitable for single-crystal X-ray diffraction (SCXRD) analysis were harvested in yields up to 20%. The newly synthesized single-crystal samples of inclusion complexes were characterized by powder X-ray diffraction (PXRD), elemental analysis, and infrared spectroscopy, confirming their phase purity, and coordination between the ligands and Cu ions, respectively (Fig. S14 and S15†).

The ^{1}H NMR spectrum of host–guest complexes in CD_2Cl_2 disclosed the host/guest ratio of 1 : 1 (Table S5†), with four sets of signals at 6.73, 3.88, 2.58 and 1.14 ppm attributed to the Cu_6L_3 host (**1**), revealing cage **1** was stable and remained intact in solution (Fig. S4†). Although the signals of guest molecules did not show noticeable downfield shifts suggesting a weak host–guest interaction and rapid guest in–out exchange in solution (Fig. S5–S12†), the guest molecules were still selectively encapsulated within the cavity of the host during the crystallization process by slowing evaporation of solvent. More interesting, the thermogravimetric measurements of single-crystal samples demonstrated that the Cu_6L_3 cages are thermally stable up to 390 °C and guests remained encapsulated up to 200 °C, far higher than the guests' boiling points, indicating guests were strongly held within the Cu_6L_3 cage in crystals (Fig. S13†).

Crystal structure determination and description

The SCXRD data for these host–guest complexes were collected with an Oxford Diffraction Gemini E instrument diffractometer or a XtaLab PRO MM007HF DW Diffractometer. In all crystals, the structure of the cage host **1** features both a hexanuclear prismatic configuration composed of two nine-membered Cu_3N_6 CTC units and three ligands (Fig. 1). Unlike the ideal planar configuration of Cu_3N_6 CTC units, in cage **1**, Cu_3N_6 rings showed a slight bending and distorted structure induced by the strong Cu_3···π interactions between the Cu_3N_6 rings and guests (Fig. 1). With the variation of guests, the distance between the center of two Cu_3N_6 rings was changed in the

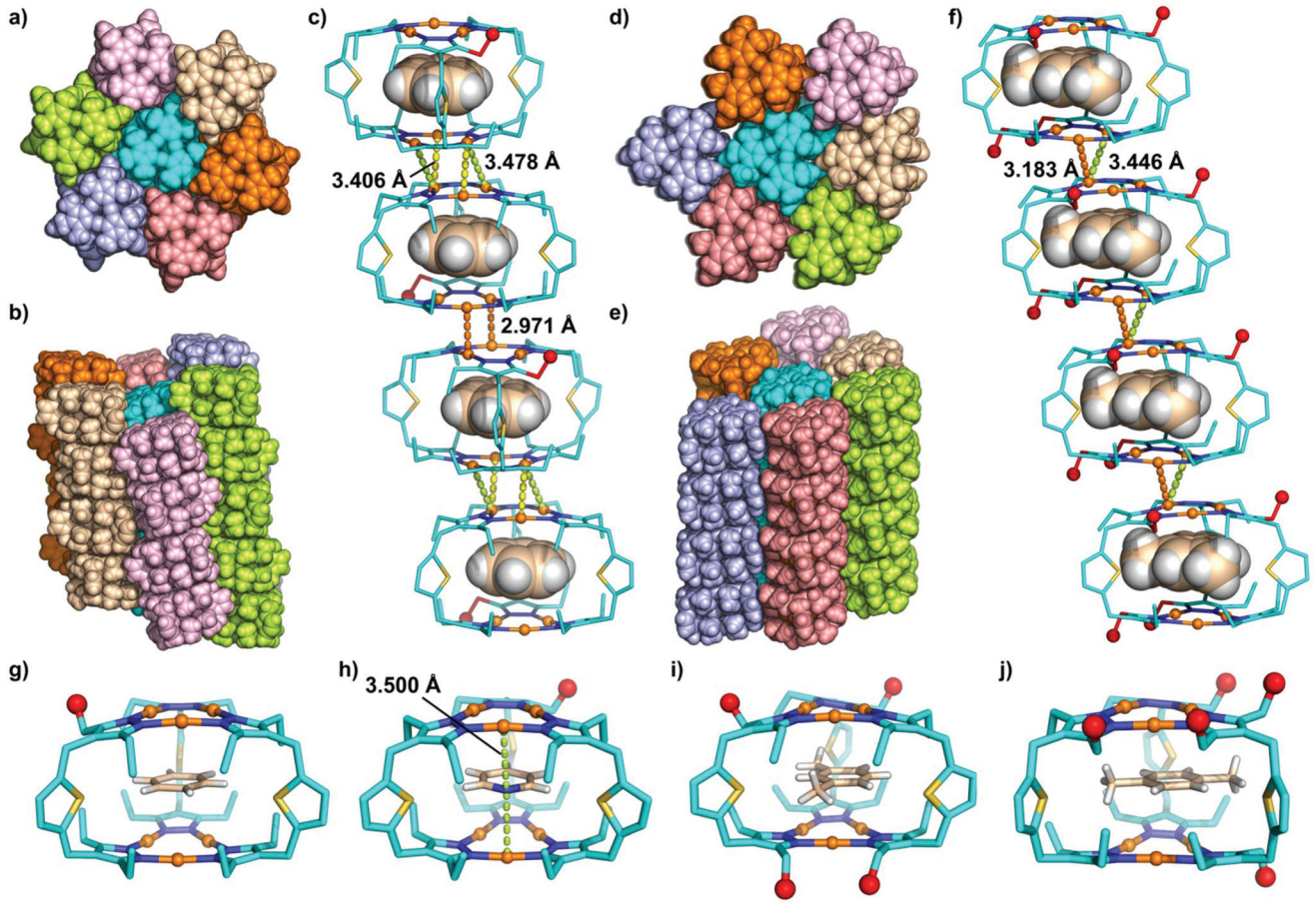

Fig. 1 Crystal structures of **1** ⊃ **Ph** and **1** ⊃ **MX**, (a) and (d) top view, and (b) and (e) side view showing the crystal packing of Cu_3L_6 cage units in **1** ⊃ **Ph** and **1** ⊃ **MX**, respectively (adjacent cage units and packed column are shown in the space-filling model with different colors; the solvent CH_3CN in **1** ⊃ **MX** is omitted for clarity); (c) and (f) The Cu_3L_6 cage units in one packed column showing the intermolecular Cu···Cu distances of 2.971, 3.406 and 3.478 Å in **1** ⊃ **Ph**, and 3.183 and 3.446 Å in **1** ⊃ **MX** (Cu(I) ions and ethyl groups flipped outward from the cage window, cage hosts **1**, and benzene guests are shown as ball, line and space-filling models, respectively; hydrogen atoms in cage hosts **1** are omitted for clarity; C, N, S, and Cu atoms in the cage are shown as cyan (to emphasize the flipped ethyl groups, their terminal carbon atoms are shown as red), blue, yellow and orange, respectively; C and H atoms in the guest are shown as wheat and white, respectively). Comparison of the asymmetric unit in the inclusion crystals of (g) **1** ⊃ **Ph**, (h) **1** ⊃ **Py**, (i) **1** ⊃ **MX**, and (j) **1** ⊃ **PX**.

range of 6.791 to 6.988 Å (Table S7†), showing no intertrimer Cu···Cu interactions within the cage,[26] and the distance between two adjacent S atoms in the ligands ranged from 9.040 to 9.250 Å approximately. Moreover, since six flexible ethyl groups can block and open up the aperture of cage **1**, the volume of the cavity is varied in the range between 218.18 $Å^3$ and 267.01 $Å^3$ with alteration of the guest, suggesting guest-induced cavity shrinking and expansion.

Single X-ray crystallographic analyses of these host–guest complexes revealed that aromatic guests were included within the cavity of the cage to form a sandwich structure and the distances between the center of the Cu_3N_6 rings and aromatic rings ranged from 3.415 to 3.980 Å, indicating existence of Cu_3···π interaction.[26] Importantly, we have found that the crystal packing can be fine-tuned by mediation of the volume occupancy, the ratio of the guest volume to the host cavity volume, which has been used to describe the molecular recognition in **ExCage** by the Stoddart group.[35] According to this approach, each inclusion complex was analyzed (Table 1) in the solid-state using Material Studio and Mercury software (see ESI† for calculation details). In our scenario, the cavity volumes of cage **1** were varied with the flipping of ethyl groups. Thus, the cavity volume of cage **1** in each inclusion complex was measured and used for calculating the percent occupancies of each aromatic guest. The values of 32.97% (**Py**), 34.71% (**Ph**), 38.41% (**Ph-Me**), 40.54% (**Ph-NO_2**), 45.70% (**OX**), 46.10% (**MX**), and 47.04% (**PX**), were obtained respectively (Table 1).

Interestingly, when the percent occupancies were in the range of 32.97 to 38.41%, only one ethyl group was flipped outward of the aperture of cage **1** in the asymmetric unit (Fig. 1g and h) and inclusion complexes of **1** ⊃ **Py**, **1** ⊃ **Ph**, and **1** ⊃ **Ph-Me** were crystallized in the same space group *P*21/*c* with a similar crystal packing mode. On the other hand,

Table 1 Summary of crystal and photophysical parameters for inclusion complexes in the solid-state

Complexes	Shortest intermolecular $d_{Cu\cdots Cu}$ (Å)	Volume occupancy (%)	Ionization potential[a] (eV)	λ_{ex} (nm)	λ_{em} (nm)	τ^c (μs) 298 K	τ^c (μs) 78 K	Φ^d (%)	$10^{-6} \times k_r{}^e$/s	$10^{-6} \times k_{nr}{}^f$/s
1 ⊃ DCM	2.796	20.04	11.35	305	643	18.53	19.76	55.5	2.995	2.402
1 ⊃ Py	2.969	32.97	9.32	340	673/580	20.33	20.80	6.9	0.339	4.579
1 ⊃ Ph	2.971	34.71	9.25	314	694	25.61	27.32	14.4	0.562	3.342
1 ⊃ Ph-Me	2.982	38.41	8.82	310	686	27.70	30.96	9.9	0.357	3.257
1 ⊃ Ph-NO$_2$[b]	3.139	40.54	—	—	—	—	—	—	—	—
1 ⊃ OX	3.043	45.70	8.56	305	659	21.08	23.44	7.4	0.351	4.393
1 ⊃ MX	3.183	46.10	8.56	313	669	19.83	19.84	6.9	0.348	4.695
1 ⊃ PX	3.793	47.04	8.45	320	636	21.15	22.57	6.8	0.321	4.407

[a] See ref. 38 and 39. [b] The photoluminescence data cannot be measured due to the guest-induced PL quenching. [c] τ is the average decay lifetime. [d] Φ was measured at 298 K. [e] Radiative decay rate constant: $k_r = \Phi/\tau$. [f] Non-radiative decay rate constant: $k_{nr} = (1 - \Phi)/\tau$.

inclusion complexes of **1 ⊃ OX**, **1 ⊃ Ph-NO$_2$**, and **1 ⊃ MX** crystallized in the space group $P\bar{1}$ with four ethyl groups flipped outward from the window of cage **1** in the asymmetric unit (Fig. 1i), when the percent occupancies were in the range of 40.54 to 46.10%. Therefore, these inclusion complexes can be divided into two categories with the one exception of **1 ⊃ PX** (*i.e.* the first category: **1 ⊃ Py**, **1 ⊃ Ph**, and **1 ⊃ Ph-Me**; the second category: **1 ⊃ OX**, **1 ⊃ Ph-NO$_2$**, and **1 ⊃ MX**).

The crystal structures of **1 ⊃ Ph** and **1 ⊃ MX** as representative examples for the first and second categories, respectively, will be discussed in detail. On one hand, the single X-ray structure of **1 ⊃ Ph** revealed that cage **1** units were stacked tightly to form a column structure *via* an intermolecular Cu⋯Cu interaction, CH/π interaction, and van der Waals forces (Fig. 1a and c) and each column was also tightly packed though van der Waals interactions (Fig. 1b). Since only one ethyl group was flipped outward from the aperture of each cage **1** unit, a strong Cu⋯Cu interaction with a short intermolecular Cu⋯Cu distance ($d_{Cu\cdots Cu}$) of 2.971 Å between two adjacent cage units in each column was observed (Fig. 1c and g). The inclusion complexes of **1 ⊃ Py** and **1 ⊃ Ph-Me** display the similar crystal packing mode to **1 ⊃ Ph**, and also exhibit short $d_{Cu\cdots Cu}$ of 2.969 and 2.982 Å, respectively (Table 1). On the other hand, the crystal structure of **1 ⊃ MX** also showed a column packing of cage **1** units, but unlike **1 ⊃ Ph**, one CH_3CN molecule was found in the asymmetric unit and interacted with the cage **1** *via* CH/π and van der Waals interactions. Importantly, four ethyl groups were flipped outward from the aperture of each cage unit, resulting in much larger steric hindrance between two adjacent cage units than that in **1 ⊃ Ph** (Fig. 1i). Therefore, a weaker Cu⋯Cu interaction and longer intermolecular Cu⋯Cu distances of 3.183 and 3.446 Å, compared to that of **1 ⊃ Ph**, were observed. In the other inclusion complexes of **1 ⊃ OX** and **1 ⊃ Ph-NO$_2$**, similar intermolecular Cu⋯Cu distances (from 3.043 to 3.689 Å) were also observed, indicating the intermolecular Cu⋯Cu distance can indeed be tuned by controlling the volume occupancy.

Although **1 ⊃ PX** crystallizes in the same space group as **1 ⊃ Ph-Me**, due to the largest guest volume and highest percent occupancy of **PX** among all the aromatic guests, five ethyl groups were flipped outward from the aperture of the cage unit (Fig. 1j), leading to the largest steric hindrance between two cage units and longest intermolecular Cu⋯Cu distances of 3.793 and 3.925 Å (Table 1). Furthermore, unlike the inclusion crystals with aromatic guests, the crystal structure of **1 ⊃ DCM** showed that two inequivalent cage units were present in the asymmetric unit and two inequivalent column structures were formed during the tight packing of cage units. The small steric hindrance and lowest percent occupancy with **DCM** led to the shortest intermolecular Cu⋯Cu distance of 2.796 Å.

To further understand the guest effects on the crystal packing, the electrostatic potential (ESP) surfaces of the inclusion complexes were calculated (see ESI† for the calculation details). The charge distribution on the surface of host **1** is significantly affected by the guest molecule (Fig. S27†). The **Py**, **Ph** and **Ph-Me** guests lead to a uniform charge distribution on the host **1** surface, resulting in relatively shorter intermolecular Cu–Cu distances. **1 ⊃ MX**, **1 ⊃ OX** and **1 ⊃ PX** display similar ESP where negative charges are enriched near the pyrazole ring of the Cu_3L_6 unit, which could induce the strong electrostatic repulsion interaction during crystal packing. The ESPs on the top and bottom surfaces of **1 ⊃ Ph-NO$_2$** are not symmetrical, the charges distributed on the three pyrazole rings within the same surface are not identical. Local electrostatic interactions might produce more complicated total intermolecular interactions. The calculated results are well consistent with the shortest intermolecular $d_{Cu\cdots Cu}$ in the crystal structure (Table 1), which further supported that the crystal packing can be fine-tuned by variation of guests.

Photoluminescence properties of inclusion complexes

The solid-state absorption spectra of the inclusion complexes illustrate that **1 ⊃ Py** and **1 ⊃ Ph-NO$_2$** show broad absorption bands in the range from 300 to 550 nm, while other inclusion complexes have absorption bands in the range from 300 to 500 nm (Fig. S16†). The charge-transfer (CT) band at 375–550 nm for **1 ⊃ Py** in the UV-vis spectrum might suggest a strong host–guest interaction. The ligand, H_2L, does not show phosphorescence in either the solid state or in CH_2Cl_2 solu-

tion. In contrast, all inclusion complexes exhibit bright luminescence upon exposure to UV irradiation and the observed lifetimes (τ) in the microsecond regime (Table 1) indicate phosphorescence. Upon cooling from room temperature to 78 K, the consistent increase in lifetime suggests a reduction in the nonradiative decay rate, as expected.

As shown in Fig. 2a, the emission spectrum of **1 ⊃ DCM** clearly exhibited an unstructured emission peak located at 643 nm at 298 K. At 78 K, it showed a broadened emission peak located at 675 nm and a structured high-energy emission band located from 450 to 550 nm which is mainly contributed to by ligand H_2L (Fig. 3a, S24 and S25†). The emission spectra of the inclusion complexes with aromatic guests at room-temperature suggest that these crystalline samples produce red phosphorescence and display a broad emission band (λ_{em}) in the range from 636 to 694 nm, while **1 ⊃ Py** exhibits orange color luminescence and dual-emission bands at 580 nm for the high-energy (HE) band and 673 nm for the low-energy (LE) band (Fig. 3a). It is worth noting that **1 ⊃ Ph-NO$_2$** is not emissive due to the electron transfer quenching mechanism and such fluorescence quenching phenomena have been commonly observed when nitroaromatic guests were used.[36]

Interestingly, variation of the aromatic guests leads to a large red shift of 58 nm (from **1 ⊃ PX** to **1 ⊃ Ph**) and the emission spectra (Fig. 2a) show a broad phosphorescence band that gradually shifts to lower energies with an increase in the electron-donating capacity of the guest molecules (Table 1). However, the emission maxima do not show a linear relationship with their ionization potentials (Fig. 2b). This might suggest that the emission is not only due to a mere charge transfer in host–guest complexes but also other mechanisms could also contribute to the luminescence. In addition, it has been reported that the emission of Cu_3Pz_3 CTC complexes is determined by the dimer rather than monomer and the main peak emission would red shift with a decrease in intermolecular Cu···Cu distance.[37] By examining the crystal packing of these inclusion complexes, we have found that the order of the $d_{Cu\cdots Cu}$ in the inclusion crystals is **1 ⊃ Ph** < **1 ⊃ Ph-Me** < **1 ⊃ MX** < **1 ⊃ OX** < **1 ⊃ PX**, which is consistent with the order of the main peak emission (694 nm for **1 ⊃ Ph**; 686 nm for **1 ⊃ Ph-Me**; 669 nm for **1 ⊃ MX**; 659 nm for **1 ⊃ OX**; 636 nm for **1 ⊃ PX**), suggesting the formation of cage stacks and short $d_{Cu\cdots Cu}$ are also responsible for the phosphorescence (Table 1). Such an observation strongly indicated that the control of aromatic guests could fine tune the photo-

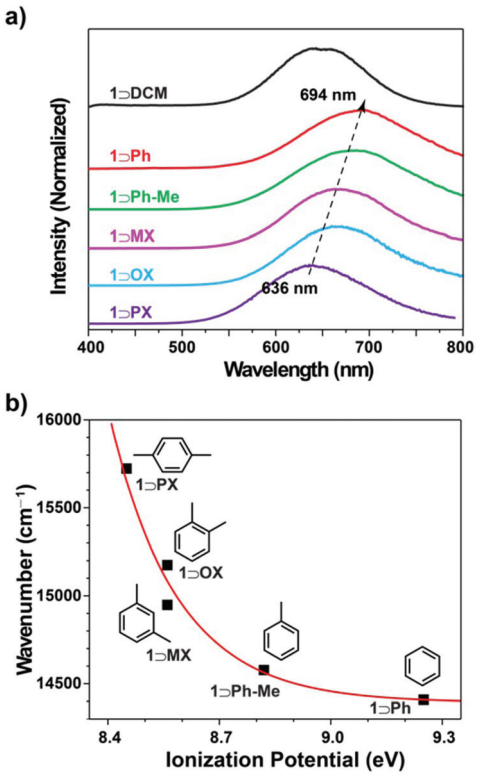

Fig. 2 (a) Intensity normalized emission spectra of inclusion complexes showing the guest-dependent red-shifted maximum emission peaks (694 nm for **1 ⊃ Ph** to 636 nm for **1 ⊃ PX**); (b) relationship between the emission maximum (cm^{-1}) and the ionization potential (eV) of the inclusion complexes.

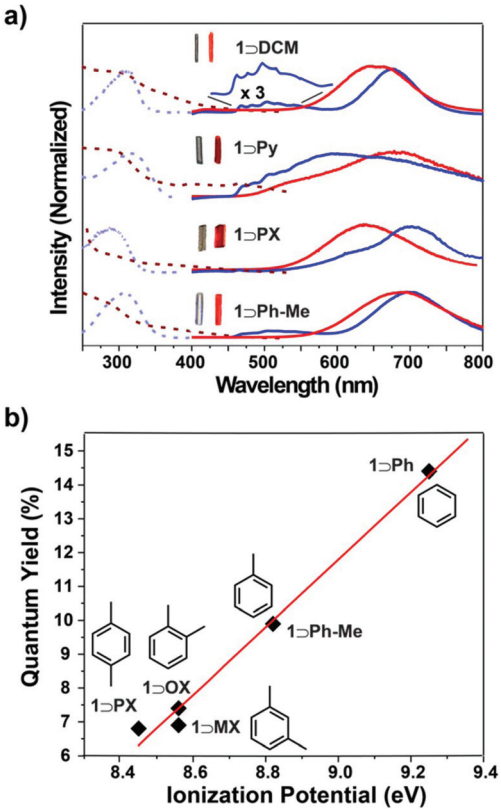

Fig. 3 (a) Representative temperature-varied emission spectra of inclusion complexes (red and blue dashed lines represent absorption and excitation spectra, respectively; red and blue solid lines represent the emission spectra at 298 and 78 K, respectively; (the inset photographs represent the inclusion crystals without (left) and with (right) exposure to UV light irradiation); (b) linear correlation between the quantum yield and ionization potential of inclusion complexes.

physical properties of inclusion complexes, which could open a new approach for designing tunable photoluminescent Cu_3Pz_3-based cage complexes.

To obtain further insights into the photophysical properties of inclusion complexes, temperature-varied emission spectra were recorded. The emission spectra of **1** ⊃ **Ph**, **1** ⊃ **Ph-Me**, **1** ⊃ **MX** and **1** ⊃ **OX** displayed similar shapes and tendencies, in which the intensity and peak position of the unstructured LE band (~636 to 694 nm) negligibly shifted with variation of temperature (Fig. S19, 20, 22 and 23†). In addition, at the low temperature of 78 K, a relatively weak and structured emission band in the HE region (~500 nm) appeared, which is similar to that observed in **1** ⊃ **DCM** and can be assigned to the emission of ligand H_2L. Unlike the others, **1** ⊃ **PX** presented one broad emission band (λ_{em} = 636 nm) at 298 K while dual-emission bands (λ_{em} = 636 and 700 nm) at 78 K (Fig. 3a), which could be attributed to the decrease in intermolecular Cu···Cu distance and the enhancing of host–guest CT at low temperature. More interestingly, **1** ⊃ **Py** showed dual-emission bands (λ_{em} = 580 and 673 nm) at 298 K, while an additional structured emission band at 450–520 nm appeared at 78 K attributed to the emission of the ligand. As shown in Fig. 1h, a short distance between the N atom and Cu (3.500 Å) was observed in the crystal of **1** ⊃ **Py**. We assumed, due to the lone pair electrons of N in **Py**, that the existence of N···Cu weak interactions may facilitate the host–guest CT process.

To further study the guest-mediated photoluminescence properties of inclusion complexes, we applied lifetime and quantum yield (QY) analysis. Radiative deactivation curves were collected at different temperatures for all samples. All inclusion complexes exhibit biexponential decay and the average emission lifetimes range from 18.53 to 27.70 μs at 298 K and 19.76 to 30.96 μs at 78 K (Table 1), suggesting phosphorescence emitting was mainly attributed to triplet, metal-to-metal charge transfer (^{3}MMCT) excited states related to the Cu···Cu interaction (cuprophilicity) of the adjacent cages. Although the encapsulation of aromatic guests was able to extend the decay lifetime compared to the non-aromatic guest (*i.e.* **DCM**), there was no simple relationship between the ionization potential and emission lifetime (Table 1). Interestingly, the QYs of inclusion complexes show a linear relationship with the guest IP (Fig. 3b), and this confirms the emission can be fine-tuned by controlling the electronic properties of guests.

Conclusions

In summary, a series of inclusion complexes, composed of a Cu_6L_3 coordination cage and various aromatic guests, was synthesized by treating a thiophene-based bispyrazolyl ligand and Cu_2O in a mixture of corresponding aromatic guests and acetonitrile. All inclusion crystals were fully characterized by NMR, powder X-ray diffraction, elemental analysis, and single-crystal X-ray diffraction. The X-ray structure analysis revealed that the intermolecular Cu···Cu distance (cuprophilicity) between two adjacent cage units can be fine-tuned by controlling the volume occupancy of the guests. When the volume occupancy increases from 32.97% for **Py** to 47.04% for **PX**, the intermolecular Cu···Cu distance extends from 2.969 Å for **Py** to 3.925 Å for **PX**. In addition, by tailoring the ionization potential of the guest, the host–guest CT interaction can be also fine-tuned. Since the photoluminescence properties of the inclusion complexes largely related to the cuprophilic interaction and the host–guest CT process, we achieved the fine-tuning of the emission properties of the inclusion crystals. For instance, (1) the maximum emission peak exhibits a red shift with the decrease in volume occupancy; (2) the quantum yield decreases with the increase in ionization potential of the guests; (3) introduction of aromatic guests can increase the emission lifetime, but it did not show a linear relationship with ionization potential. These examples of mediating the phosphorescence properties of coordination cages may open a new approach for designing tunable phosphorescence meta-organic cage complexes.

Conflicts of interest

There are no conflicts to declare.

Acknowledgements

This work was financially supported by the National Natural Science Foundation of China (No. 21731002, 21975104, 21871172, and 21701049), the China Postdoctoral Science Foundation (2018M633272, 2017M622894) and Jinan University. G.-H. Ning thanks for the financial support from Guangdong Basic and Applied Basic Research Foundation (2019B151502024), Guangdong Province Pearl River Scholar Funded Scheme (2019), and the Fundamental Research Funds for the Central Universities (21619315).

Notes and references

1 M. Fujita, Metal-directed self-assembly of two- and three-dimensional synthetic receptors, *Chem. Soc. Rev.*, 1998, **27**, 417–425.
2 S. Leininger, B. Olenyuk and P. J. Stang, Self-Assembly of Discrete Cyclic Nanostructures Mediated by Transition Metals, *Chem. Rev.*, 2000, **100**, 853–908.
3 D. L. Caulder and K. N. Raymond, Supermolecules by Design, *Acc. Chem. Res.*, 1999, **32**, 975–982.
4 T. R. Cook and P. J. Stang, Recent Developments in the Preparation and Chemistry of Metallacycles and Metallacages via Coordination, *Chem. Rev.*, 2015, **115**, 7001–7045.
5 D. Zhang, T. K. Ronson and J. R. Nitschke, Functional Capsules via Subcomponent Self-Assembly, *Acc. Chem. Res.*, 2018, **51**, 2423–2436.

6 Y. Inokuma, M. Kawano and M. Fujita, Crystalline molecular flasks, *Nat. Chem.*, 2011, **3**, 349–358.

7 M. L. Saha, X. Yan and P. J. Stang, Photophysical Properties of Organoplatinum(II) Compounds and Derived Self-Assembled Metallacycles and Metallacages: Fluorescence and its Applications, *Acc. Chem. Res.*, 2016, **49**, 2527–2539.

8 K. Ono, J. K. Klosterman, M. Yoshizawa, K. Sekiguchi, T. Tahara and M. Fujita, ON/OFF Red Emission from Azaporphine in a Coordination Cage in Water, *J. Am. Chem. Soc.*, 2009, **131**, 12526–12527.

9 X. Yan, T. R. Cook, P. Wang, F. Huang and P. J. Stang, Highly emissive platinum(II) metallacages, *Nat. Chem.*, 2015, **7**, 342–348.

10 Z. Zhou, D.-G. Chen, M. K. Saha, H. Wang, X. Li, P.-T. Chou and P. J. Stang, Designed Conformation and Fluorescence Properties of Self-Assembled Phenazine-Cored Platinum(II) Metallacycles, *J. Am. Chem. Soc.*, 2019, **141**, 5535–5543.

11 P. R. Neelakandan, A. Jiménez and J. R. Nitschke, Fluorophore incorporation allows nanomolar guest sensing and white-light emission in M_4L_6 cage complexes, *Chem. Sci.*, 2014, **5**, 908–915.

12 D. Asil, J. A. Foster, A. Patra, X. de Hatten, J. del Barrio, O. A. Scherman, J. R. Nitschke and R. H. Friend, Temperature- and Voltage-Induced Ligand Rearrangement of a Dynamic Electroluminescent Metallopolymer, *Angew. Chem., Int. Ed.*, 2014, **53**, 8388–8391.

13 W. J. Ramsay, F. T. Szczypiński, H. Weissman, T. K. Ronson, M. M. J. Smulders, B. Rybtchinski and J. R. Nitschke, Designed Enclosure Enables Guest Binding Within the 4200 $Å^3$ Cavity of a Self-Assembled Cube, *Angew. Chem., Int. Ed.*, 2015, **54**, 5636–5640.

14 K. Mahata, P. D. Frischmann and F. Würthner, Giant Electroactive M_4L_6 Tetrahedral Host Self-Assembled with Fe(II) Vertices and Perylene Bisimide Dye Edges, *J. Am. Chem. Soc.*, 2013, **135**, 15656–15661.

15 W. Xuan, M. Zhang, Y. Liu, Z. Chen and Y. Cui, A Chiral Quadruple-Stranded Helicate Cage for Enantioselective Recognition and Separation, *J. Am. Chem. Soc.*, 2012, **134**, 6904–6907.

16 D. Luo, M. Li, X.-P. Zhou and D. Li, Boosting Luminescence of Planar-Fluorophore-Tagged Metal–Organic Cages Via Weak Supramolecular Interactions, *Chem. – Eur. J.*, 2018, **24**, 7108–7113.

17 C.-L. Liu, R.-L. Zhang, C.-S. Lin, L.-P. Zhou, L.-X. Cai, J.-T. Kong, S.-Q. Yang, K.-L. Han and Q.-F. Sun, Intraligand Charge Transfer Sensitization on Self-Assembled Europium Tetrahedral Cage Leads to Dual-Selective Luminescent Sensing toward Anion and Cation, *J. Am. Chem. Soc.*, 2017, **139**, 12474–12479.

18 R. V. Slone, J. T. Hupp, C. L. Stern and T. E. Albrecht-Schmitt, Self-Assembly of Luminescent Molecular Squares Featuring Octahedral RheniumCorners, *Inorg. Chem.*, 1996, **35**, 4096–4097.

19 L. E. Kreno, K. Leong, O. K. Farha, M. Allendorf, R. P. Van Duyne and J. T. Hupp, Metal–Organic Framework Materials as Chemical Sensors, *Chem. Rev.*, 2012, **112**, 1105–1125.

20 N. K. Al-Rasbi, C. Sabatini, F. Barigelletti and M. D. Ward, Red-shifted luminescence from naphthalene-containing ligands due to π-stacking in self-assembled coordination cages, *Dalton Trans.*, 2006, 4769–4772.

21 J. R. Shakirova, E. V. Grachova, V. V. Gurzhiy, S. K. Thangaraj, J. J. Janis, A. S. Melnikov, A. J. Karttunen, S. P. Tunik and I. O. Koshevoy, Heterometallic Cluster-Capped Tetrahedral Assemblies with Postsynthetic Modification of the Metal Cores, *Angew. Chem., Int. Ed.*, 2018, **57**, 14154–14158.

22 S. Goeb, V. Prusakova, X. Wang, A. Vézinat, M. Sallé and F. N. Castellano, Phosphorescent self-assembled Pt^{II} tetranuclear metallocycles, *Chem. Commun.*, 2011, **47**, 4397–4399.

23 (*a*) S. J. Lee, C. R. Luman, F. N. Castellano and W. Lin, Directed assembly of chiral organometallic squares that exhibit dual luminescence, *Chem. Commun.*, 2003, 2124–2125; (*b*) L. Zhang, Y.-H. Niu, A. K. Y. Jen and W. Lin, A highly electroluminescent molecular square, *Chem. Commun.*, 2005, 1002–1004.

24 J. Yang, M. Bhadbhade, W. A. Donald, H. Iranmanesh, E. G. Moore, H. Yan and J. E. Beves, Self-assembled supramolecular cages containing ruthenium(II) polypyridyl complexes, *Chem. Commun.*, 2015, **51**, 4465–4468.

25 Y. Zhang, M. R. Crawley, C. E. Hauke, A. E. Friedman and T. R. Cook, Phosphorescent Decanuclear Bimetallic Pt_6M_4 (M = Zn, Fe) Tetrahedral Cages, *Inorg. Chem.*, 2017, **56**, 4258–4262.

26 M. A. Omary, M. A. Rawashdeh-Omary, M. W. A. Gonser, O. Elbjeirami, T. Grimes, T. R. Cundari, H. V. K. Diyabalanage, C. S. P. Gamage and H. V. R. Dias, Metal Effect on the Supramolecular Structure, Photophysics, and Acid–Base Character of Trinuclear Pyrazolato Coinage Metal Complexes, *Inorg. Chem.*, 2005, **44**, 8200–8210.

27 H. V. R. Dias, H. V. K. Diyabalanage, M. G. Eldabaja, O. Elbjeirami, M. A. Rawashdeh-Omary and M. Omary, Brightly Phosphorescent Trinuclear Copper(I) Complexes of Pyrazolates: Substituent Effects on the Supramolecular Structure and Photophysics, *J. Am. Chem. Soc.*, 2005, **127**, 7489–7501.

28 H. Yang, J. Zheng, S. Peng, X. Zhu, M. Wan, W. Lu and D. Li, A chemopalette strategy for white light by modulating monomeric and excimeric phosphorescence of a simple Cu(I) cyclic trinuclear unit, *Chem. Commun.*, 2019, **55**, 4635–4638.

29 T. Jozak, Y. Sun, Y. Shmitt, S. Lebedkin, M. Kappes and W. R. Thiel, New Hexanuclear Group 11 Pyrazolate Complexes: Synthesis and Photophysical Features, *Chem. – Eur. J.*, 2011, **17**, 3384–3389.

30 G.-F. Gao, M. Li, S.-Z. Zhan, Z. Lv, G.-H. Chen and D. Li, Confined Metallophilicity within a Coordination Prism, *Chem. – Eur. J.*, 2011, **17**, 4113–4117.

31 Z.-C. Shi, D.-X. Zhang, S.-Z. Zhan, M. Li, J. Zheng, H. Yang, X.-P. Zhou and D. Li, Trigonal Prismatic Cu_6L_3 Coordination Cage: Encapsulation of Aromatic Molecules

and Tuned Photoluminescence, *Isr. J. Chem.*, 2019, **59**, 317–322.

32 J. Zheng, H. Yang, M. Xie and D. Li, The π-acidity/basicity of cyclic trinuclear units (CTUs): from a theoretical perspective to potential applications, *Chem. Commun.*, 2019, **55**, 7134–7146.

33 S. M. Tekarli, T. R. Cundari and M. Omary, Rational Design of Macrometallocyclic Trinuclear Complexes with Superior π-Acidity and π-Basicity, *J. Am. Chem. Soc.*, 2008, **130**, 1669–1675.

34 (*a*) R. Hahn, F. Bohle, W. Fang, A. Walther, S. Grimme and B. Esser, Raising the Bar in Aromatic Donor–Acceptor Interactions with Cyclic Trinuclear Gold(I) Complexes as Strong π-Donors, *J. Am. Chem. Soc.*, 2018, **140**, 17932–17944; (*b*) R. Hahn, F. Bohle, S. Kotte, T. J. Keller, S.-S. Jester, A. Hansen, S. Grimme and B. Esser, Donor–acceptor interactions between cyclic trinuclear pyridinate gold(I)-complexes and electron-poor guests: nature and energetics of guest-binding and templating on graphite, *Chem. Sci.*, 2018, **9**, 3477–3483.

35 E. J. Dale, N. A. Vermeulen, A. A. Thomas, J. C. Barnes, M. Juríček, A. K. Blackburn, N. L. Strutt, A. A. Sarjeant, C. L. Stern, S. E. Denmark and J. F. Stoddart, ExCage, *J. Am. Chem. Soc.*, 2014, **136**, 10669–10682.

36 S. J. Toala and W. C. Trogler, Polymer sensors for nitroaromatic explosives detection, *J. Mater. Chem.*, 2006, **16**, 2871–2883.

37 B. Hu, G. Gahungu and J. Zhang, Optical Properties of the Phosphorescent Trinuclear Copper(I) Complexes of Pyrazolates: Insights from Theory, *J. Phys. Chem. A*, 2007, **111**, 4965–4973.

38 Y. Takashima, V. M. Martínez, S. Furukawa, M. Kondo, S. Shimomura, H. Uehara, M. Nakahama, K. Sugimoto and S. Kitagawa, Molecular decoding using luminescence from an entangled porous framework, *Nat. Commun.*, 2011, **2**, 168.

39 G. Andric, J. F. Boas, A. M. Bond, G. D. Fallon, K. P. Ghiggino, C. F. Hogan, J. A. Hutchison, M. A.-P. Lee, S. J. Langford, J. R. Pilbrow, G. J. Troup and C. P. Woodward, Spectroscopy of Naphthalene Diimides and Their Anion Radicals, *Aust. J. Chem.*, 2004, **57**, 1011–1019.

